

Article

An Upper Bound Solution for Axisymmetric Extrusion and Drawing Considering a Generalized Yield Criterion

Sergei Alexandrov ^{1,2,3} , Stanislav Strashnov ⁴  and Yong Li ^{2,*}¹ Ishlinsky Institute for Problems in Mechanics RAS, 101-1 Prospect Vernadskogo, Moscow 119526, Russia² School of Mechanical Engineering and Automation, Beihang University, No. 37 Xueyuan Road, Beijing 100191, China³ Department of Civil Engineering, Peoples' Friendship University of Russia (RUDN University), 6 Miklukho-Maklaya St., Moscow 117198, Russia⁴ General Education Courses Department, Peoples' Friendship University of Russia (RUDN University), 6 Miklukho-Maklaya St., Moscow 117198, Russia

* Correspondence: liyong19@buaa.edu.cn

Abstract: The yield criterion of many metallic materials differs from the von Mises yield criterion. However, the available upper bound solutions are almost all restricted to this criterion. The objective of the present paper was to derive an upper bound solution based on a generalized yield criterion for evaluating the extrusion and drawing force, assuming a conical die. The solution method differs from the conventional method used in conjunction with the von Mises yield criterion. The development of this method is necessary, since the work function is not readily expressed as an explicit function of strain rate invariants if the generalized yield criterion is adopted. The solution is illustrated using numerical examples, which show the effect of the yield criterion on the limit load.

Keywords: extrusion; drawing; generalized yield criterion; upper bound; singularity



Citation: Alexandrov, S.; Strashnov, S.; Li, Y. An Upper Bound Solution for Axisymmetric Extrusion and Drawing Considering a Generalized Yield Criterion. *Metals* **2023**, *13*, 602. <https://doi.org/10.3390/met13030602>

Academic Editor: Mohammad Jahazi

Received: 20 January 2023

Revised: 14 March 2023

Accepted: 15 March 2023

Published: 16 March 2023



Copyright: © 2023 by the authors. Licensee MDPI, Basel, Switzerland. This article is an open access article distributed under the terms and conditions of the Creative Commons Attribution (CC BY) license (<https://creativecommons.org/licenses/by/4.0/>).

1. Introduction

The upper bound technique is often used to evaluate the loads required for performing metal formation processes. The general theorem is available for quite a large class of constitutive equations [1]. However, its application is almost exclusively restricted to the von Mises yield criterion. In this case, the work function introduced in [1] can readily be expressed as an explicit function of the quadratic invariant of the strain rate tensor.

Pioneering solutions for axisymmetric extrusion and drawing through conical dies have been provided in [2,3]. These solutions are based on simple radial kinematically admissible velocity fields, without parameters for minimization. These fields include two spherical velocity discontinuity surfaces between the plastic region and two rigid blocks moving along the axis of symmetry. The paper in [4] extended these solutions [2,3], assuming that these velocity discontinuity surfaces are not spherical. The equations determining these surfaces may include several parameters for minimization. Paper [5] clarified that an additional rigid region may appear near the friction surface. As a result, an additional velocity discontinuity surface appears. Paper [6] employed the kinematically admissible velocity field proposed in [4] to account for the singular behavior of the real velocity field near the maximum friction surfaces. Note that this singular behavior is valid for a large class of yield criteria, not only for the von Mises yield criterion [7]. A continuous kinematically admissible velocity field for axisymmetric extrusion and drawing through conical dies was proposed in [8].

The solutions above were extended to non-conical dies in [9–13]. The mean yield criterion was adopted in [13]. A mathematical feature of this criterion is that the work function introduced in [1] can readily be expressed as an explicit function of the principal strain rates. Therefore, the use of this criterion in conjunction with the upper bound

theorem does not differ from the use of the von Mises yield criterion. Meanwhile, many yield criteria that adequately describe the behavior of various materials do not exhibit such a mathematical feature. Particular forms of such yield criteria were proposed in [14,15].

The extrusion and drawing processes have also been extensively used in methods other than the upper bound theorem. The effect of temperature and speed on the drawing force in the wire drawing process was studied in [16]. Automatic optimization techniques were employed in [17] to determine the optimal die angle in wire drawing. The relationships between the various kinematic parameters in plane-strain drawing were derived in [18]. The effect of the die geometry on the drawing force was studied in [19], using three-dimensional finite element simulation. Finite element simulation was used in [20–22] to show the influence of various parameters on the wire-drawing process. An experimental study on the effect of elastic deformation in the material entering the plastic region on the drawing force was conducted in [23].

The present paper adopts the yield criterion proposed in [14] to reveal the effect of a parameter involved in this criterion on the extrusion and drawing forces. Moreover, the effect of process parameters on these forces is shown for several values of this parameter. These values correspond to BCC and FCC metals. The solution's novelty is that this yield criterion has not previously been used in conjunction with the upper bound theorem. Moreover, the solution accounts for the singular behavior of the real velocity field near maximum friction surfaces [7].

2. Statement of the Problem

A schematic diagram of extrusion and drawing processes through a conical die is shown in Figure 1. The initial radius of the rod is R_0 , and its final radius is R_1 . The die angle is 2α . In addition, $F_d = 0$ in the case of extrusion, and $F_e = 0$ in the case of drawing. The velocity of the rod entering the plastic region is V_0 . The velocity of the rod existing from the plastic region is V_1 . Estimating F_d in the case of drawing and F_e in the case of extrusion is required. It is natural to use the spherical coordinate system (ρ, θ, φ) shown in Figure 1. The solution is independent of φ .

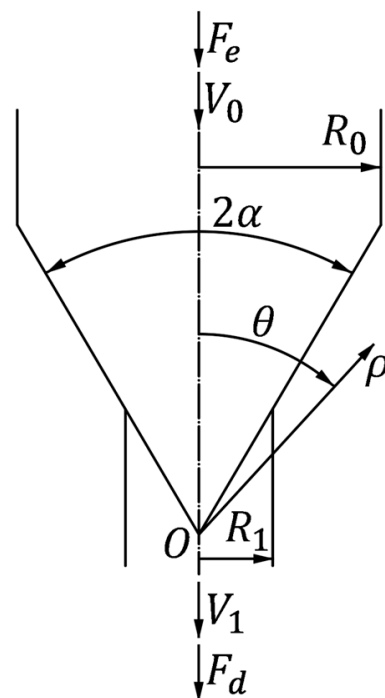


Figure 1. Schematic diagram of the extrusion and drawing processes.

The material is assumed to be rigid and perfectly plastic. An essential difference with the available solutions is that it obeys the generalized yield criterion proposed in [14]. In terms of the principal stresses σ_1 , σ_2 , and σ_3 , this criterion reads

$$(\sigma_1 - \sigma_2)^n + (\sigma_2 - \sigma_3)^n + (\sigma_1 - \sigma_3)^n = 2\sigma_0^n, \quad (1)$$

where σ_0 is the yield stress in tension and n is constant. The yield criterion in the form of (1) is based on the assumption

$$\sigma_1 \geq \sigma_2 \geq \sigma_3. \quad (2)$$

The plastic flow rule associated with the yield criterion (1) is

$$\begin{aligned} \zeta_1 &= \chi n \left[(\sigma_1 - \sigma_2)^{n-1} + (\sigma_1 - \sigma_3)^{n-1} \right], \\ \zeta_2 &= -\chi n \left[(\sigma_1 - \sigma_2)^{n-1} + (\sigma_3 - \sigma_2)^{n-1} \right], \\ \zeta_3 &= \chi n \left[(\sigma_3 - \sigma_2)^{n-1} - (\sigma_1 - \sigma_3)^{n-1} \right]. \end{aligned} \quad (3)$$

Here ζ_1 , ζ_2 , and ζ_3 are the principal strain rates and $\chi \geq 0$. Additionally, the principal directions of the stress and strain rate tensors coincide. It is seen from (1) that the shear yield stress is

$$k = \frac{\sigma_0}{\sqrt[n]{1 + 2^{n-1}}}. \quad (4)$$

The die surface is rough. The friction law is assumed to be $\tau_f = mk$, where τ_f is the friction stress and $0 \leq m \leq 1$. Using (4), one can represent this law as

$$\tau_f = \frac{m}{\sqrt[n]{1 + 2^{n-1}}} \sigma_0 \quad (5)$$

for $\theta = \alpha$.

3. Kinematically Admissible Velocity Field

The boundary value problem is axisymmetric. Therefore, it is sufficient to consider a generic meridian plane. In the remainder of this paper, the velocity discontinuity surfaces will be referred to as the velocity discontinuity lines, meaning the intersections of the generic meridian plane and the velocity discontinuity surfaces.

The kinematically admissible velocity field proposed in [4] can be combined with any pressure-independent yield criterion. The present section outlines the basic equations required when using the upper bound theorem. It is convenient to introduce the following dimensionless quantities:

$$\mu = \frac{\rho^2}{R_0^2} \text{ and } \lambda = \frac{R_0^2}{R_1^2}. \quad (6)$$

The general structure of the kinematically admissible velocity field is shown in Figure 2. The material above line AB and below line A'B' is rigid. These rigid blocks move along the axis of symmetry. The velocity field in the plastic region ABB'A' must be compatible with these motions. It is assumed that the only non-vanishing velocity component in the plastic region is the radial velocity in the spherical coordinate system (Figures 1 and 2). This velocity component is represented as

$$u_\rho = -\frac{V_0 u(\theta)}{\mu}, \quad (7)$$

where $u(\theta) > 0$ is an arbitrary function of θ . It is straightforward to check that the velocity field chosen satisfies the equation of incompressibility. In particular, the non-vanishing strain rate components in the spherical coordinate system are

$$\zeta_{\rho\rho} = \frac{2V_0u(\theta)}{R_0\mu^{3/2}}, \zeta_{\theta\theta} = \zeta_{\varphi\varphi} = -\frac{V_0u(\theta)}{R_0\mu^{3/2}}, \zeta_{\rho\theta} = -\frac{V_0}{2R_0\mu^{3/2}} \frac{du}{d\theta}. \tag{8}$$

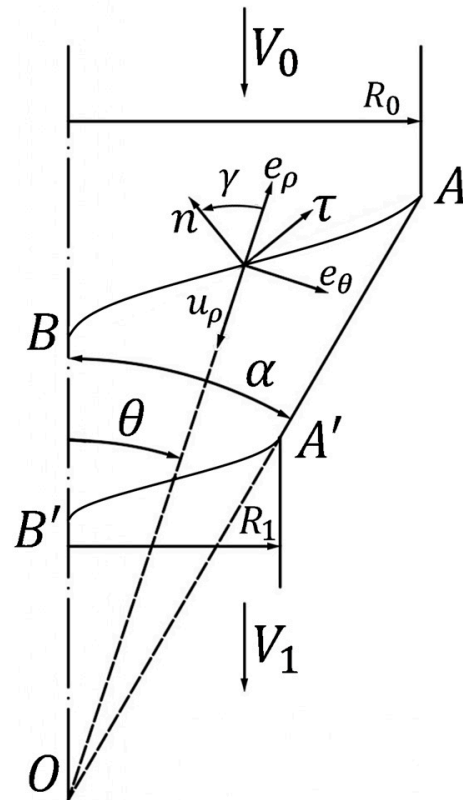


Figure 2. General structure of the kinematically admissible velocity field chosen.

Consider the rigid/plastic boundary AB (Figure 2). Let \mathbf{n} and $\boldsymbol{\tau}$ be unit vectors normal and tangent to this boundary, respectively. The vector \mathbf{n} makes angle γ with the radial coordinate, measured from the coordinate line anticlockwise. In addition, \mathbf{e}_ρ and \mathbf{e}_θ are the unit base vectors of the spherical coordinate system. It follows from the geometry of Figure 2 that

$$\mathbf{n} = \cos \gamma \mathbf{e}_\rho - \sin \gamma \mathbf{e}_\theta \text{ and } \boldsymbol{\tau} = \sin \gamma \mathbf{e}_\rho + \cos \gamma \mathbf{e}_\theta. \tag{9}$$

The velocity vectors in the rigid and plastic regions are given by

$$\mathbf{u}_r = -V_0(\cos \theta \mathbf{e}_\rho - \sin \theta \mathbf{e}_\theta) \text{ and } \mathbf{u}_p = u_\rho \mathbf{e}_\rho, \tag{10}$$

respectively. The continuity of the normal velocity across the velocity discontinuity line demands $\mathbf{u}_r \cdot \mathbf{n} = \mathbf{u}_p \cdot \mathbf{n}$ on AB. Using (7), (9), and (10), one can transform this equation to

$$\frac{u(\theta)}{\mu} - \cos \theta - \tan \gamma \sin \theta = 0. \tag{11}$$

It follows from the geometry of Figure 2 and (6) that

$$\frac{1}{2\mu} \frac{d\mu}{d\theta} = \tan \gamma. \tag{12}$$

Eliminating $\tan \gamma$ in (11) employing (12), one can obtain

$$\frac{d\mu}{d\theta} = \frac{2}{\sin \theta} (u - \mu \cos \theta). \quad (13)$$

Since $\rho = R_0/\sin \alpha$ and $\theta = \alpha$ at A, it follows from (6) that

$$\mu = \frac{1}{\sin^2 \alpha} \quad (14)$$

for $\theta = \alpha$. The solution of Equation (13) satisfying boundary condition (14) is

$$\mu = \mu_{AB}(\theta) = \frac{1}{\sin^2 \theta} \left[2 \int_{\alpha}^{\theta} u(\eta) \sin \eta d\eta + 1 \right]. \quad (15)$$

This curve may have a common point with the axis of symmetry only if

$$\int_0^{\alpha} u(\theta) \sin \theta d\theta = \frac{1}{2}. \quad (16)$$

In the following, it is assumed that the function $u(\theta)$ is chosen to satisfy this condition. Then, applying l'Hospital's rule, one can find from (15) that

$$u = \mu \quad (17)$$

at $\theta = 0$.

The amount of velocity jump across AB is required to apply the upper bound theorem. By definition, this amount is given by

$$[u] = |(\mathbf{u}_r - \mathbf{u}_p) \cdot \boldsymbol{\tau}|. \quad (18)$$

Substituting (7), (9), (10), and (13) into (18) yields

$$[u] = V_0 \frac{\sin \theta}{\cos \gamma}. \quad (19)$$

An infinitesimal surface element of AB is given by

$$dS = \rho \sqrt{\left(\frac{d\rho}{\rho d\theta}\right)^2 + 1} \sin \theta d\theta d\varphi. \quad (20)$$

Employing (6) and (12), one can transform this equation into

$$dS = R_0^2 \frac{\mu \sin \theta}{\cos \gamma} d\theta d\varphi. \quad (21)$$

The velocity discontinuity line $A'B'$ (Figure 2) can be treated similarly. In particular, the equation of this line is

$$\mu = \mu_{A'B'}(\theta) = \frac{1}{\lambda \sin^2 \theta} \left[2 \int_{\alpha}^{\theta} u(\eta) \sin \eta d\eta + 1 \right]. \quad (22)$$

The kinematically admissible velocity field is classified using three parameters: λ , α , and V_0 . However, the latter is immaterial, because the material model is rate independent.

4. Estimation of Extrusion and Drawing Forces

The upper bound theorem for an arbitrary yield criterion was proven in [1,24]. The theorem [1] involves the work function, which is a function of the invariants of the strain rate tensor. In the case of the von Mises yield criterion, the work function is a linear function of the quadratic invariant. This simplicity is the reason for using the von Mises yield criterion in almost all upper bound solutions. In the case of the yield criterion (1), the work function cannot readily be expressed as an explicit function of the invariants, except for some particular n -values. Therefore, one must consider Equation (3) together with a kinematically admissible velocity field.

The plastic work rate in the plastic region is

$$W_V = 2\pi \int_0^\alpha \int_{\rho_{A'B'}(\theta)}^{\rho_{AB}(\theta)} (\zeta_1\sigma_1 + \zeta_2\sigma_2 + \zeta_3\sigma_3)\rho^2 \sin\theta d\rho d\theta. \tag{23}$$

Here $\rho = \rho_{AB}(\theta)$ and $\rho = \rho_{A'B'}(\theta)$ are the equations of the velocity discontinuity lines AB and $A'B'$, respectively (Figure 2). Using (6), one can rewrite this equation as

$$\frac{W_V}{\pi R_0^2 V_0 \sigma_0} = \frac{1}{\sigma_0} \int_0^\alpha \int_{\mu_{A'B'}(\theta)}^{\mu_{AB}(\theta)} (\varepsilon_1\sigma_1 + \varepsilon_2\sigma_2 + \varepsilon_3\sigma_3) \sin\theta d\mu d\theta, \tag{24}$$

where

$$\varepsilon_1 = \zeta_1 \frac{R_0}{V_0}, \varepsilon_2 = \zeta_2 \frac{R_0}{V_0}, \text{ and } \varepsilon_3 = \zeta_3 \frac{R_0}{V_0}. \tag{25}$$

The limits $\mu_{AB}(\theta)$ and $\mu_{A'B'}(\theta)$ are given by Equations (15) and (22). Equation (8) allows for the principal strain rates to be calculated. Then, it follows from (25) that

$$\varepsilon_1 = \frac{1}{2\mu^{3/2}} \left(\Lambda + \sqrt{9\Lambda^2 + \Lambda_1^2} \right), \varepsilon_2 = \frac{1}{2\mu^{3/2}} \left(\Lambda - \sqrt{9\Lambda^2 + \Lambda_1^2} \right), \varepsilon_3 = -\frac{u(\theta)}{\mu^{3/2}}, \tag{26}$$

where

$$\Lambda(\theta) = \mu \cos\theta + \frac{\sin\theta}{2} \frac{d\mu}{d\theta} \text{ and } \Lambda_1(\theta) = \frac{\sin\theta}{2} \frac{d^2\mu}{d\theta^2} + \frac{3\cos\theta}{2} \frac{d\mu}{d\theta} - \mu \sin\theta. \tag{27}$$

Introduce the following stress variables:

$$s_{12} = \frac{\sigma_1 - \sigma_2}{\sigma_0}, s_{13} = \frac{\sigma_1 - \sigma_3}{\sigma_0}, \text{ and } s_{32} = \frac{\sigma_3 - \sigma_2}{\sigma_0}. \tag{28}$$

It is evident that

$$s_{12} - s_{32} - s_{13} = 0. \tag{29}$$

Equation (1) becomes

$$s_{12}^n + s_{23}^n + s_{13}^n = 2. \tag{30}$$

Equations (3), (25), and (28) yield

$$\eta = \frac{\varepsilon_1}{\varepsilon_2} = -\frac{s_{12}^{n-1} + s_{13}^{n-1}}{s_{12}^{n-1} + s_{32}^{n-1}}. \tag{31}$$

On the other hand, the first two equations in (26) result in

$$\eta(\theta) = \frac{\Lambda + \sqrt{9\Lambda^2 + \Lambda_1^2}}{\Lambda - \sqrt{9\Lambda^2 + \Lambda_1^2}}. \tag{32}$$

Equations (31) and (32) combine to give

$$-\frac{s_{12}^{n-1} + s_{13}^{n-1}}{s_{12}^{n-1} + s_{32}^{n-1}} = \frac{\Lambda + \sqrt{9\Lambda^2 + \Lambda_1^2}}{\Lambda - \sqrt{9\Lambda^2 + \Lambda_1^2}}. \quad (33)$$

Equations (29), (30), and (33) constitute the system for determining s_{12} , s_{13} , and s_{32} as functions of θ . In particular,

$$s_{12} = \sqrt[n]{\frac{2}{1 + A^n + (1 - A)^n}}, \quad s_{32} = A s_{12}, \quad \text{and} \quad s_{13} = s_{12} - s_{32}, \quad (34)$$

where $A(\theta)$ is determined from the equation

$$\eta A^{n-1} + (1 - A)^{n-1} + 1 + \eta = 0. \quad (35)$$

This equation should be solved numerically. The principal stresses are determined from (28). Then, upon substitution of these stresses, (6), and (26) into (24), one finds

$$\frac{W_V}{\pi R_0^2 V_0 \sigma_0} = \frac{\ln \lambda}{2} \int_0^\alpha (s_{13} \eta - s_{32}) \left[\Lambda - \sqrt{9\Lambda^2 + \Lambda_1^2} \right] \sin \theta d\theta. \quad (36)$$

This integral should be evaluated numerically.

The plastic work rate dissipated at the velocity discontinuity surface AB (Figure 2) is

$$W_d = k \int_S [u] dS, \quad (37)$$

where $[u]$ and dS are given by (19) and (21), respectively. Using these equations and (4), one can rewrite (37) as

$$\frac{W_d}{\pi R_0^2 V_0 \sigma_0} = \frac{2}{\sqrt[n]{1 + 2^{n-1}}} \int_0^\alpha \mu \frac{\sin^2 \theta}{\cos^2 \gamma} d\theta. \quad (38)$$

In this equation, γ can be eliminated using (12). Then, the integral involved in (38) can be evaluated numerically.

The plastic work rate dissipated at the velocity discontinuity surface $A'B'$ (Figure 2) is calculated similarly. In particular, since $V_0 R_0^2 = V_1 R_1^2$, this work rate equals W_d .

The plastic work rate dissipated at the friction surface is

$$W_f = \tau_f \int_S |[u]| dS, \quad (39)$$

where $[u]$ equals the radial velocity at $\theta = \alpha$ and $dS = \rho \sin \alpha d\phi d\rho$. Using (5), (6), and (7), one can rewrite (39) as

$$\frac{W_f}{\pi R_0^2 V_0 \sigma_0} = \frac{m \sqrt[n]{1 + 2^{n-1}} \sin \alpha u(\alpha)}{3} \int_{1/(\lambda \sin^2 \alpha)}^{1/\sin^2 \alpha} \frac{d\mu}{\mu} = \frac{m \sin \alpha u(\alpha) \ln \lambda}{\sqrt[n]{1 + 2^{n-1}}}. \quad (40)$$

The virtual work-rate principle for a continuum yields

$$F_e V_0 = W_V + 2W_d + W_f \quad \text{and} \quad F_d V_1 = W_V + 2W_d + W_f \quad (41)$$

for extrusion and drawing, respectively. Using (36), (38), (40), and (41), and employing the upper bound theorem [24], one can derive

$$f_u = \frac{\ln \lambda}{2} \int_0^\alpha (s_{13}\eta - s_{32}) \left[\Lambda - \sqrt{9\Lambda^2 + \Lambda_1^2} \right] \sin \theta d\theta + \frac{4}{\sqrt[n]{1 + 2^{n-1}}} \int_0^\alpha \mu \frac{\sin^2 \theta}{\cos^2 \gamma} d\theta + \frac{m \sin \alpha u(\alpha) \ln \lambda}{\sqrt[n]{1 + 2^{n-1}}}. \quad (42)$$

Here f_u is an upper bound on the dimensionless extrusion force, defined as $f_e = F_e / (\pi R_0^2 \sigma_0)$. Since $V_0 R_0^2 = V_1 R_1^2$, it is straightforward to show that f_u is also an upper bound on the dimensionless drawing force defined as $f_d = F_d / (\pi R_1^2 \sigma_0)$.

It remains to assume $u(\theta)$ or $\mu(\theta)$. It is more convenient to specify $\mu(\theta)$ and find $u(\theta)$ from (13). It is known that the velocity field is singular near the friction surface if $m = 1$ [7]. In this case, the function must contain a term of order $O[(\alpha - \theta)^{3/2}]$ as $\theta \rightarrow \alpha$. The function proposed in [6] is

$$\mu(\theta) = \frac{1}{\sin^2 \alpha} + b(\alpha - \theta)^{3/2}. \quad (43)$$

This function satisfies (14) at any value of b . It follows from (13) and (43) that

$$u(\theta) = -\frac{3b}{4} \sqrt{\alpha - \theta} \sin \theta + \frac{\cos \theta}{\sin^2 \alpha} + b \cos \theta (\alpha - \theta)^{3/2}. \quad (44)$$

This function satisfies (16) at any value of b . Equations (43) and (44) allow for the integrands and the last term in (42) to be calculated. The right-hand side of this equation should be minimized with respect to b , to find the best upper bound limit load based on the kinematically admissible velocity field chosen.

If $b \rightarrow 0$, the kinematically admissible velocity field chosen reduces to that used in [3]. In this case, the upper bound limit load is determined from (42) with no minimization. Its value coincides with the solution [3], which confirms the correctness of the derivation of (42).

A rigid region may appear near the friction surface if the angle α is large [5]. This new rigid plastic boundary is a velocity discontinuity line. The equation of this line is $\theta = \beta$, where

$$\beta \leq \alpha \quad (45)$$

Equation (42) is valid, but α should be replaced with β , and it is necessary to use $m = 1$. As a result,

$$f_u = \frac{\ln \lambda}{2} \int_0^\beta (s_{13}\eta - s_{32}) \left[\Lambda - \sqrt{9\Lambda^2 + \Lambda_1^2} \right] \sin \theta d\theta + \frac{4}{\sqrt[n]{1 + 2^{n-1}}} \int_0^\beta \mu \frac{\sin^2 \theta}{\cos^2 \gamma} d\theta + \frac{\sin \beta u(\beta) \ln \lambda}{\sqrt[n]{1 + 2^{n-1}}}. \quad (46)$$

It is also necessary to replace α with β in (43) and (44). The right-hand side of (46) should be minimized with respect to b and β , to find the best upper bound limit load based on the kinematically admissible velocity field chosen. Equation (45) should be taken into account in the course of minimization.

The main output of the solution is the dimensionless extrusion or drawing force. In addition, the solution determines whether or not a rigid region appears near the friction surface. If it does, the other important output parameter is the angle β . The essential input parameters are λ , α , n , and m .

5. Numerical Examples

Using numerical integration and minimization, one can estimate the extrusion and drawing force from (42) or (46). The present section provides several numerical examples. A comprehensive parametric analysis has not been performed, because of the many parameters required. Moreover, using commercially available software, it is straightforward to carry out the numerical operations above for any given set of parameters.

5.1. Drawing

In the case of drawing, both α and m are small. Typical values of these and other process parameters are provided, for example, in [25]. The dependence of the dimensionless drawing force on n at several values of α is depicted in Figure 3. These calculations were carried out using (42) at $m = 0.05$ and $\lambda = 1.07$. Figure 3 demonstrates the effect of the yield criterion on the drawing force. Figures 4 and 5 demonstrate the effect of α on this force at $\lambda = 1.07$ and several n -values. These calculations were carried at $m = 0.05$ and $m = 0.15$, respectively. Note that $n = 2$ corresponds to the von Mises yield criterion. Moreover, the yield criterion (1) closely approximates the yield criteria for BCC and FCC metals if $n = 6$ and $n = 8$, respectively [26]. Tresca's yield criterion is approaching when $n \rightarrow \infty$.

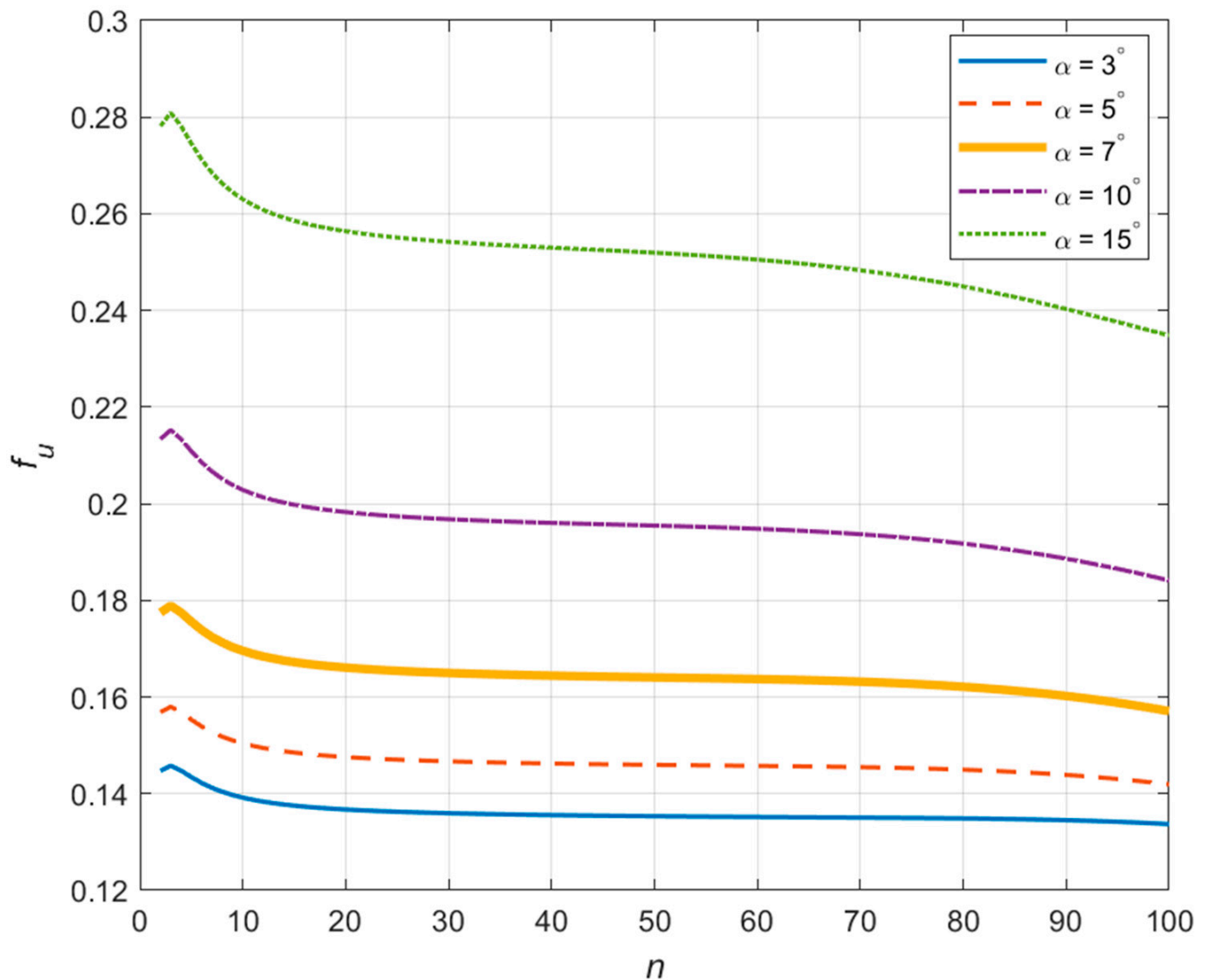


Figure 3. Variation of the dimensionless drawing force with n at several die semi-angles α . The value of n controls the shape of the yield surface.

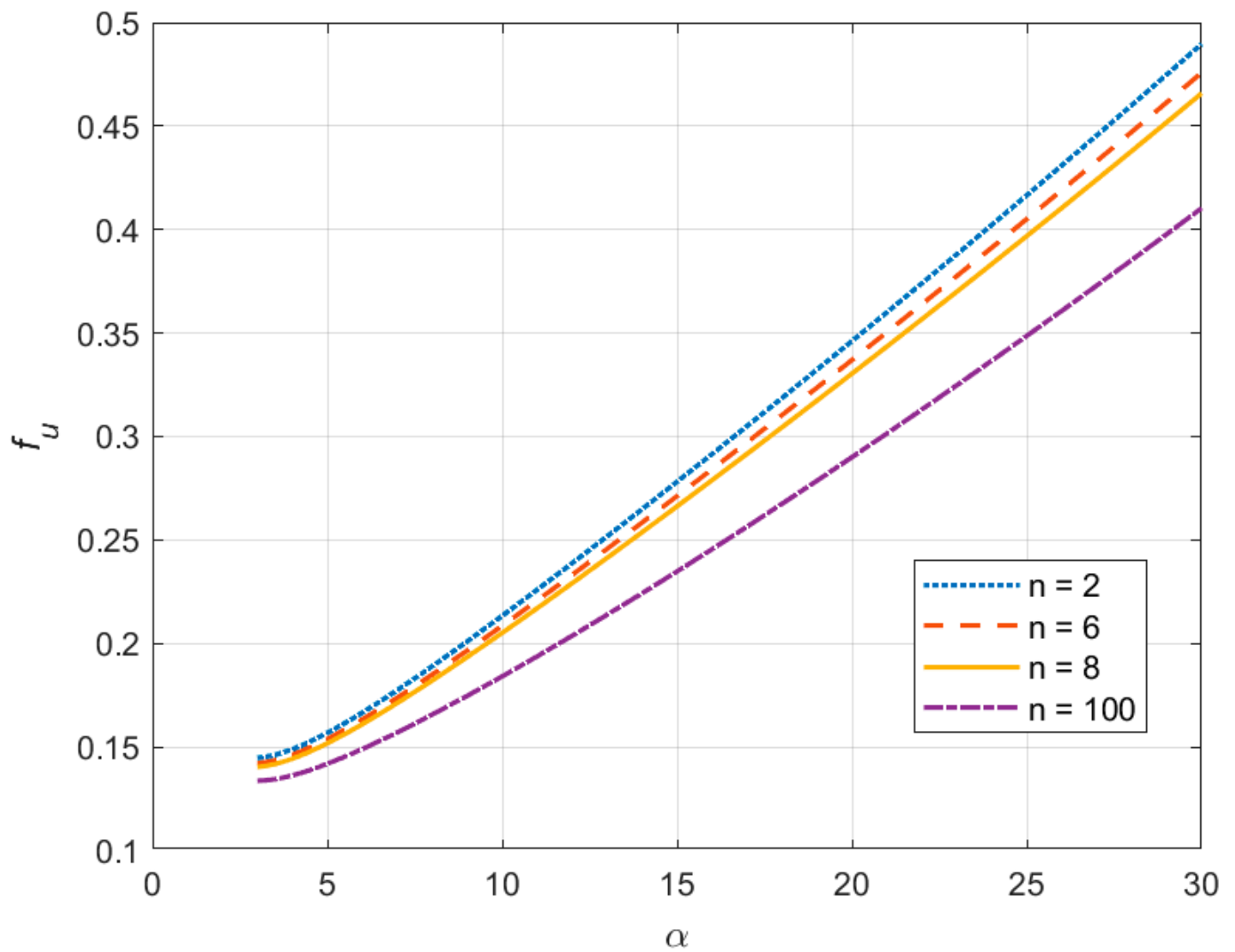


Figure 4. Variation of the dimensionless drawing force with the die's semi-angle at $m = 0.05$ and several n -values. The values of m and n control the friction stress and the shape of the yield surface, respectively.

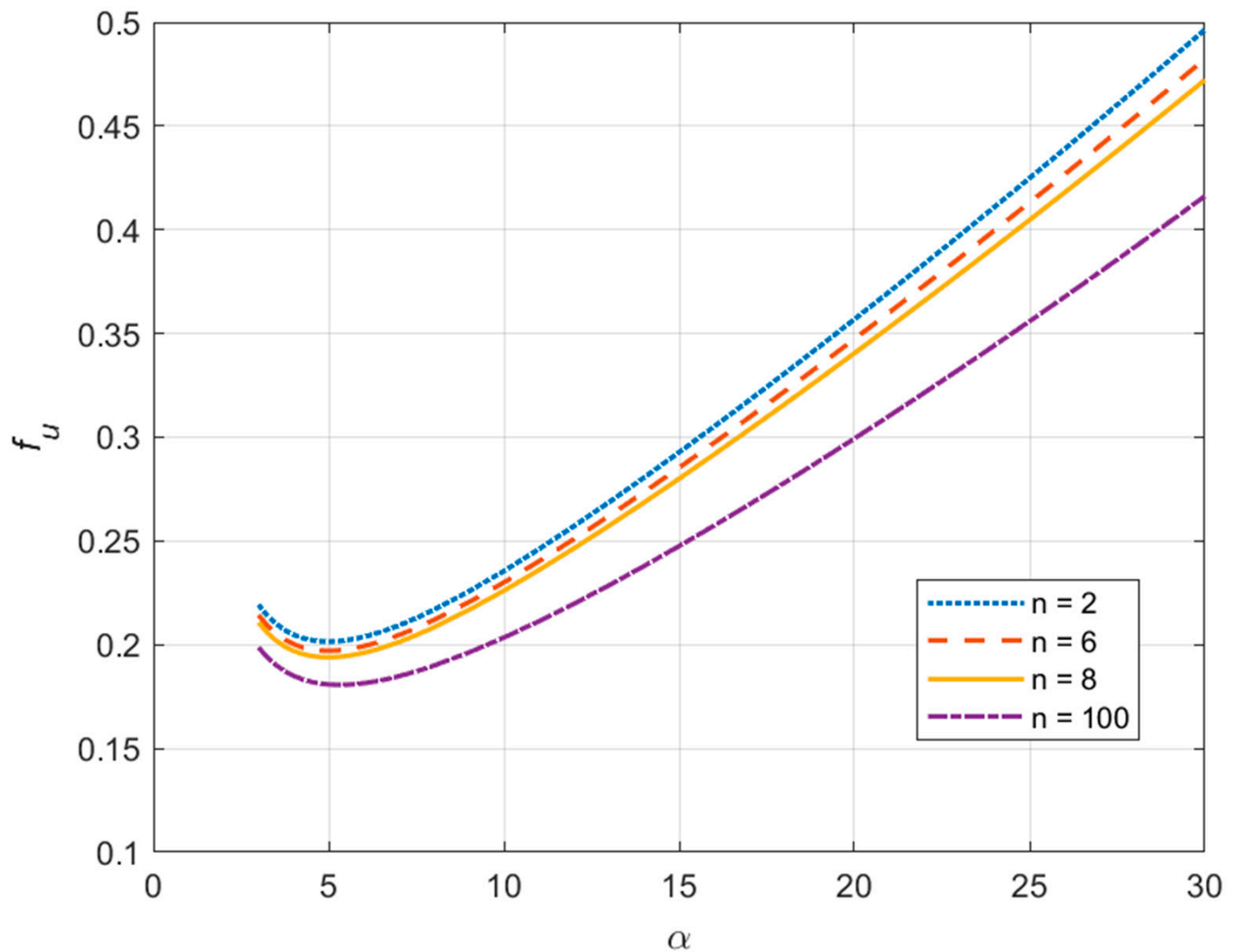


Figure 5. Variation of the dimensionless drawing force with die's semi-angle at $m = 0.15$ and several n -values. The values of m and n control the friction stress and the shape of the yield surface, respectively.

5.2. Extrusion

In the case of extrusion, the angle α may be so large that a rigid region appears near the friction surface [5]. Therefore, Equation (46) should be used to determine the extrusion force. The dependence of the dimensionless extrusion force on n at several values of λ is depicted in Figure 6. This figure demonstrates the effect of the yield criterion on the extrusion force. The inequality in (45) determines the range of validity of this solution if $m = 1$ at the friction surface. The variation of β with n is depicted in Figure 7.

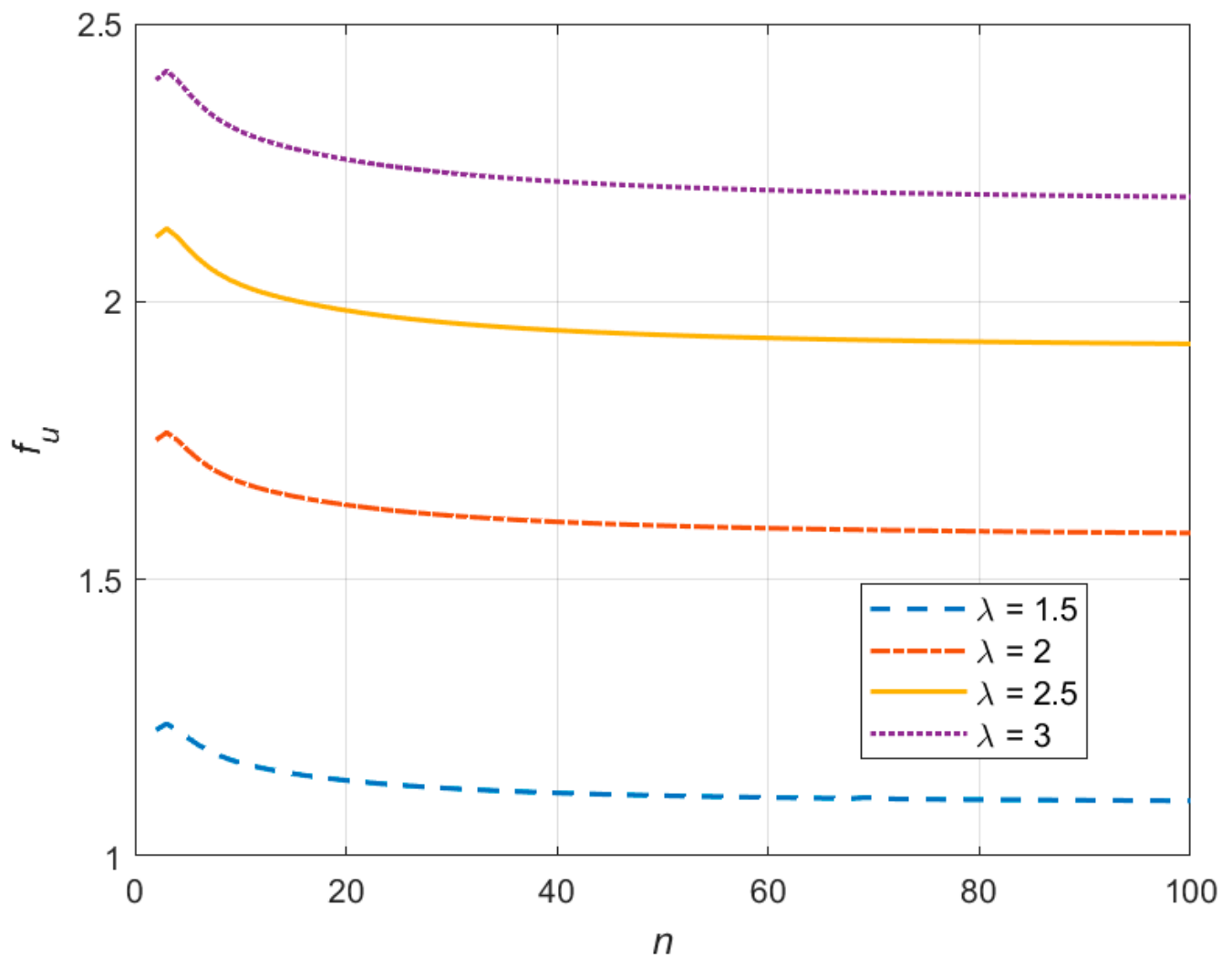


Figure 6. Variation of the dimensionless extrusion force with n at several extrusion ratios, λ . The value of n controls the shape of the yield surface.

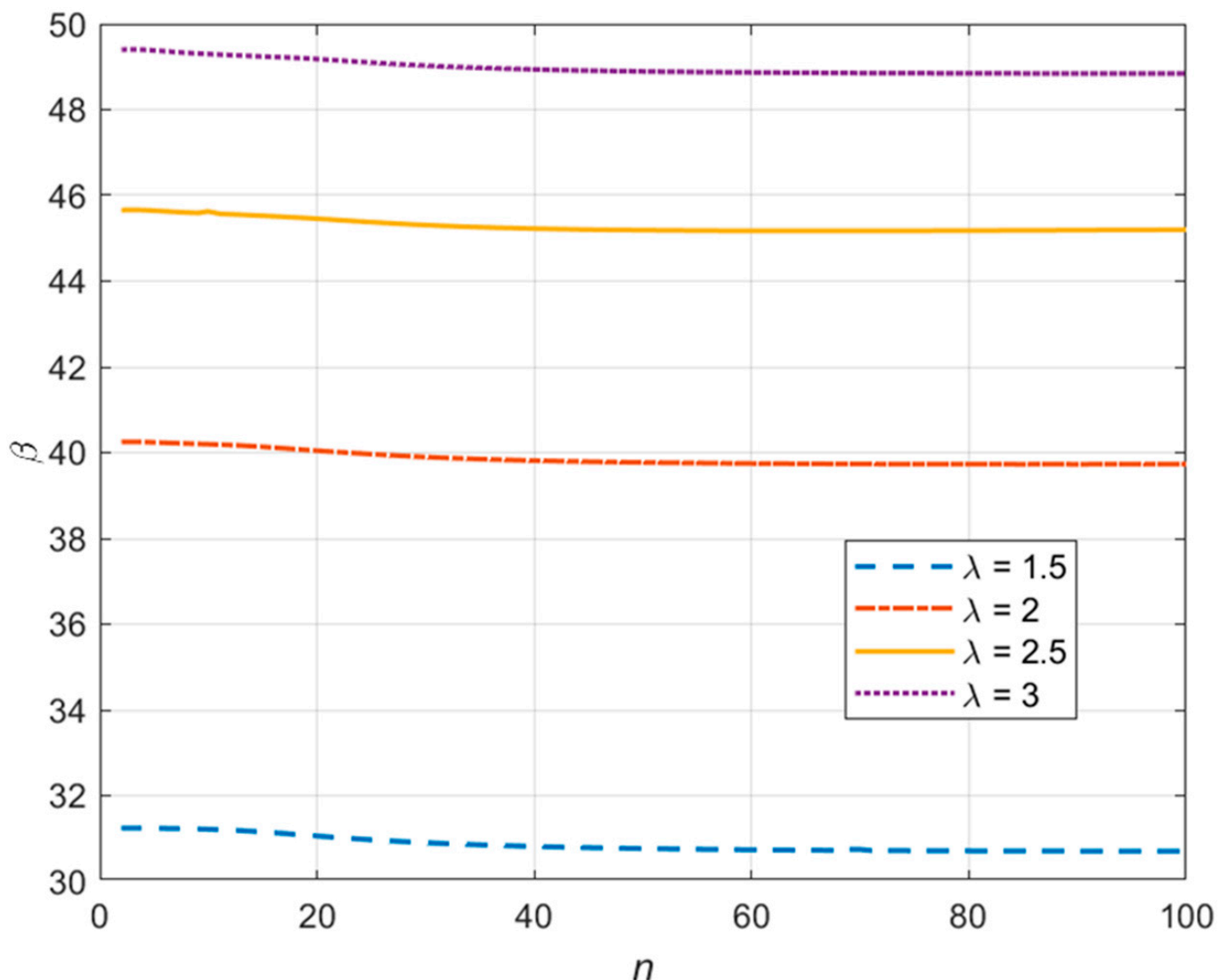


Figure 7. Variation of β with n at several extrusion ratios, λ . The value of n controls the shape of the yield surface. The angle β determines the rigid plastic boundary between the plastic region and the rigid region appearing near the friction surface.

6. Discussion

A new upper bound solution for extrusion and drawing through a conical die has been found. Its outstanding feature over the available upper bound solutions is that the yield criterion proposed in [14] has been adopted. A difficulty with using this yield criterion in conjunction with the upper bound theorem is that the plastic work rate is not readily expressed as an explicit function of the strain rate invariants. The solution accounts for the singular behavior of the real velocity field near maximum friction surfaces and the possibility of the appearance of a rigid region near the friction surface.

Numerical integration and minimization are required to evaluate the extrusion (or drawing) force using Equations (42) or (46). The latter accounts for a rigid region near the friction surface, and the former does not.

The numerical results have been collected in Section 5. These results illustrate the effect of the yield criterion on the limit load. Particular values of the exponent n in Figures 4 and 5 correspond to the von Mises yield criterion ($n = 2$), BCC metals ($n = 6$), FCC metals ($n = 8$), and a nearly Tresca yield criterion ($n = 100$). Figure 7 shows the effect of the yield criterion on the size of a rigid region that appears near the friction surface.

7. Conclusions

The main achievement of the present paper is that it provides a procedure for finding upper bound solutions in the case of arbitrary pressure-independent yield criteria and applies this procedure to evaluate the extrusion and drawing forces in the case of conical dies.

Author Contributions: Formal analysis, S.A. and S.S.; conceptualization, Y.L.; supervision, Y.L.; writing—original draft, S.A. and S.S. All authors have read and agreed to the published version of the manuscript.

Funding: This research was supported by the Foreign Expert Project from the Ministry of Science and Technology of China (G2022177004L).

Institutional Review Board Statement: Not applicable.

Informed Consent Statement: Not applicable.

Data Availability Statement: Not applicable.

Acknowledgments: This paper was supported by the RUDN University Strategic Academic Leadership Program.

Conflicts of Interest: The authors declare no conflict of interest.

References

1. Hill, R. New Horizons in the Mechanics of Solids. *J. Mech. Phys. Solids* **1956**, *5*, 66–74. [\[CrossRef\]](#)
2. Avitzur, B. Analysis of Wire Drawing and Extrusion Through Conical Dies of Small Cone Angle. *J. Eng. Ind.* **1963**, *85*, 89–95. [\[CrossRef\]](#)
3. Avitzur, B. Analysis of Wire Drawing and Extrusion Through Conical Dies of Large Cone Angle. *J. Eng. Ind.* **1964**, *86*, 305–314. [\[CrossRef\]](#)
4. Osakada, K.; Niimi, Y. A Study on Radial Flow Field for Extrusion through Conical Dies. *Int. J. Mech. Sci.* **1975**, *17*, 241–254. [\[CrossRef\]](#)
5. Tirosch, J. On the Dead-Zone Formation in Plastic Axially-Symmetric Converging Flow. *J. Mech. Phys. Solids* **1971**, *19*, 39–47. [\[CrossRef\]](#)
6. Alexandrov, S.; Mishuris, G.; Miszuris, W.; Sliwa, R.E. On the Dead-Zone Formation and Limit Analysis in Axially Symmetric Extrusion. *Int. J. Mech. Sci.* **2001**, *43*, 367–379. [\[CrossRef\]](#)
7. Alexandrov, S.; Richmond, O. Singular Plastic Flow Fields near Surfaces of Maximum Friction Stress. *Int. J. Non Linear Mech.* **2001**, *36*, 1–11. [\[CrossRef\]](#)
8. Lambert, E.R.; Kobayashi, S. A Theory on the Mechanics of Axisymmetric Extrusion through Conical Dies. *J. Mech. Eng. Sci.* **1968**, *10*, 367–380. [\[CrossRef\]](#)
9. Yang, D.Y.; Han, C.H.; Lee, B.C. The Use of Generalised Deformation Boundaries for the Analysis of Axisymmetric Extrusion through Curved Dies. *Int. J. Mech. Sci.* **1985**, *27*, 653–663. [\[CrossRef\]](#)
10. Yang, D.Y.; Han, C.H. A New Formulation of Generalized Velocity Field for Axisymmetric Forward Extrusion Through Arbitrarily Curved Dies. *J. Eng. Ind.* **1987**, *109*, 161–168. [\[CrossRef\]](#)
11. Gordon, W.A.; Van Tyne, C.J.; Sriram, S. Extrusion Through Spherical Dies—An Upper Bound Analysis. *J. Manuf. Sci. Eng.* **2002**, *124*, 92–97. [\[CrossRef\]](#)
12. Chang, D.-F.; Wang, J. Optimized Upper Bound Analysis of Axisymmetric Extrusion Using Spherical Velocity Field. *J. Manuf. Sci. Eng.* **2006**, *128*, 4–10. [\[CrossRef\]](#)
13. Zhang, S.H.; Chen, X.D.; Zhou, J.; Zhao, D.W. Upper Bound Analysis of Wire Drawing through a Twin Parabolic Die. *Meccanica* **2016**, *51*, 2099–2110. [\[CrossRef\]](#)
14. Hosford, W.F. A Generalized Isotropic Yield Criterion. *J. Appl. Mech.* **1972**, *39*, 607–609. [\[CrossRef\]](#)
15. Billington, E.W. Generalized Isotropic Yield Criterion for Incompressible Materials. *Acta Mech.* **1988**, *72*, 1–20. [\[CrossRef\]](#)
16. Haddi, A.; Imad, A.; Vega, G. Analysis of temperature and speed effects on the drawing stress for improving the wire drawing process. *Mater. Des.* **2011**, *32*, 4310–4315. [\[CrossRef\]](#)
17. Massé, T.; Fourment, L.; Montmitonnet, P.; Bobadilla, C.; Foissey, S. The optimal die semi-angle concept in wire drawing, examined using automatic optimization techniques. *Int. J. Mater. Form.* **2013**, *6*, 377–389. [\[CrossRef\]](#)
18. Dobrov, I.V. On kinematics-of stock deformation process during drawing. *Procedia Eng.* **2017**, *206*, 760–770. [\[CrossRef\]](#)
19. Sas-Boca, I.M.; Tintelecan, M.; Pop, M.; Iluțiu-Varvara, D.-A.; Mihiu, A.M. The Wire Drawing Process Simulation and the Optimization of Geometry Dies. *Procedia Eng.* **2017**, *181*, 187–192. [\[CrossRef\]](#)
20. Martinez, G.A.S.; Santos, E.F.D.; Kabayama, L.K.; Guidi, E.S.; Silva, F.D.A. Influences of Different Die Bearing Geometries on the Wire-Drawing Process. *Metals* **2019**, *9*, 1089. [\[CrossRef\]](#)

21. Martinez, G.A.S.; Qian, W.-L.; Kabayama, L.K.; Prisco, U. Effect of Process Parameters in Copper-Wire Drawing. *Metals* **2020**, *10*, 105. [[CrossRef](#)]
22. Strzpek, P.; Mamala, A.; Zasadzińska, M.; Kiesiewicz, G.; Knych, T.A. Shape analysis of the elastic deformation region throughout the axi-symmetric wire drawing process of ETP grade copper. *Materials* **2021**, *14*, 4713. [[CrossRef](#)] [[PubMed](#)]
23. Strzpek, P.; Mamala, A.; Zasadzińska, M.; Nowak, A. Extensive analysis of the ETP grade copper wire drawing force parameters in correlation with the length of the elastic deformation region. *Metalurgija* **2022**, *61*, 634–636.
24. Prager, W.; Hodge, P.G. *Theory of Perfectly Plastic Solids*; J. Wiley & Sons, Inc.: New York, NY, USA, 1951.
25. Alexandrov, S.; Hwang, Y.-M.; Tsui, H.S.R. Determining the Drawing Force in a Wire Drawing Process Considering an Arbitrary Hardening Law. *Processes* **2022**, *10*, 1336. [[CrossRef](#)]
26. Alexandrov, S.; Barlat, F. Modeling Axisymmetric Flow through a Converging Channel with an Arbitrary Yield Condition. *Acta Mech.* **1999**, *133*, 57–68. [[CrossRef](#)]

Disclaimer/Publisher's Note: The statements, opinions and data contained in all publications are solely those of the individual author(s) and contributor(s) and not of MDPI and/or the editor(s). MDPI and/or the editor(s) disclaim responsibility for any injury to people or property resulting from any ideas, methods, instructions or products referred to in the content.